2023-07

Optimization Approaches for Intensity Modulated Proton Therapy Treatment Planning

Mousazadeh, Bahar

UNIVERSITY OF CALGARY

Optimization Approaches for Intensity Modulated Proton Therapy Treatment Planning

by

Bahar Mousazadeh

A THESIS

SUBMITTED TO THE FACULTY OF GRADUATE STUDIES

IN PARTIAL FULFILMENT OF THE REQUIREMENTS FOR THE

DEGREE OF MASTER OF SCIENCE

GRADUATE PROGRAM IN MATHEMATICS AND STATISTICS

CALGARY, ALBERTA

JULY, 2023

Abstract

Radiation therapy is a critical modality in the field of oncology. The primary goal of radiation therapy is to destroy or control the growth of cancerous cells while minimizing damage to healthy tissues. Intensity Modulated Proton Therapy (IMPT) is a type of radiation therapy that utilizes protons to irradiate the tumor. The unique physical properties of protons enable precise control over the radiation dose distribution within the tumor and more effective sparing of healthy tissues. Typically, radiation therapy treatment planning is posed as a multi-criteria optimization problem, whereby the challenge is finding the best possible treatment plan. In this study, we formulate and compare two optimization approaches for IMPT treatment planning. We first explore a linear programming (LP) approach, followed by a moment-based approach where we incorporate the dose-volume requirements into the fluence map optimization (FMO) problem. The evaluation of these models is conducted using anonymized patient data corresponding to a lung cancer case, with a focus on generating a good-quality initial plan that is amenable to further refinement. The moment-based approach has a drawback in terms of its high memory usage. To mitigate this limitation, we explore several sparsification strategies aimed at reducing memory requirements. Employing an aggressive sparsification method, we demonstrate that the moment-based approach outperforms the LP model in dosimetric outcomes and computational run-time. We highlight a trade-off between the quality of the treatment plan and computational run-time when utilizing different sparcification strategies for the moment-based approach. By adopting a less strict sparsification method, we anticipate achieving higher-quality treatment plans at the expense of increased computational run-time.

Preface

This thesis is an original work by the author under the supervision of Dr. Yuriy Zinchenko. No part of this thesis has been previously published.

Acknowledgements

I would like to express my sincerest gratitude to my supervisor, Dr. Yuriy Zinchenko, for his invaluable guidance and insightful feedback. His continuous support and encouragement have helped me exceed my expectations and played a crucial role in shaping my academic and professional growth.

I am grateful to our collaborators at the University of Lehigh and the University of Pennsylvania for providing me with the necessary resources to conduct this research. Their expertise, insights, and invaluable contributions have significantly enriched the outcomes of this study.

Finally, I would like to express my heartfelt appreciation to my family for their encouragement and unwavering support during my academic journey.

To my beloved family ...

Table of Contents

List of Figures

List of Tables

List of Symbols, Abbreviations, and Nomenclature

Symbol	Definition
IMPT	Intensity Modulated Proton Therapy
LP	Linear Programming
FMO	Fluence Map Optimization
IMRT	Intensity Modulated Radiation Therapy
DNA	Deoxyribonucleic Acid
CT	Computed Tomography
MRI	Magnetic Resonance Imaging
TPS	Treatment Planning System
OAR	Organ at Risk
DVH	Dose-Volume Histogram
PTV	Planning Target Volume
cGy	Centigray
Gy	Gray
MIP	Mixed Integer Programming
gEUD	Generalized Equivalent Uniform Dose
GTV	Gross Tumor Volume
CTV	Clinical Target Volume
RS	Range Shifter
DICOM	Digital Imaging and Communications in Medicine

GUI	Graphical User Interface
VOI	Volume of Interest
IPOPT	Interior Point Optimizer Package
SOCP	Second-Order Conic Programming

Chapter 1

Introduction

In Canada, cancer accounts for 28.2% of all deaths. It was estimated that in 2022, 233,900 people would be diagnosed with cancer, 85,100 of whom would die from this disease [3]. There are different methods for treating cancer, including surgery, chemotherapy, and radiation therapy. One or a combination of two treatment procedures is chosen for each patient, depending on the type and stage of cancer [4].

1.1 Radiation Therapy

Radiation therapy is a ubiquitous treatment for several types of cancer. There are two types of radiation therapy, namely external (beam) radiation therapy and internal radiation therapy. In internal radiation therapy, radioactive materials are placed in the body, whereas in external radiation therapy, a machine directs high-energy beams to the point in the body where the tumor lies. In this study, we will focus on external radiation therapy. Various techniques are used to deliver external radiation therapy, including Intensity Modulated Radiation Therapy (IMRT) and Intensity Modulated Proton Therapy (IMPT). IMRT is an advanced approach where the radiation intensity is tailored to match the target's shape. Moreover, the intensity of each individual beam can vary, resulting in the delivery of a higher radiation dose to the tumor while minimizing the radiation dose to adjacent healthy

tissues. IMPT uses protons instead of traditional radiation such as X-ray. We will discuss the differences between the two approaches in Section 1.6. The radiation damages the deoxyribonucleic acid (DNA) of cancerous cells, stopping them from growing and dividing [5]. An inevitable side effect of this treatment is that the radiation can damage healthy tissues as it passes through the body. Therefore, the objective of radiation therapy is to minimize the damage to healthy tissues while destroying or shrinking the tumor.

1.2 Treatment planning

After being diagnosed with cancer, the radiation therapist orders imaging tests such as a computed tomography (CT) scan or magnetic resonance imaging (MRI) based on the type of cancer. The information collected from these tests is imported into a treatment planning system (TPS) and is used to build the treatment plan for the patient. The treatment plan specifies the intensity of the radiation beams that are delivered to the patient's body during each treatment session.

Typically, radiation therapy treatment planning is posed as a multi-criteria optimization problem. Depending on the type of cancer and where the tumor lies, the medical physicist collaborates with the radiation oncologist to determine the dose distribution for both the target and the organs at risk (OAR). An OAR refers to a healthy organ that is close to the target. The objective function and the constraints are defined to meet the desired dose distribution. After the optimization problem is solved and the beam intensities are obtained, the dose distribution for each organ is computed and compared using dose-volume histograms (DVH) to the desired dose distribution defined before planning. We will talk more about the DVH in Section 1.4. This comparison determines the quality of the plan. The closer the resulting dose distribution is to the desired dose, the higher the quality of the treatment plan.

1.3 Dose-Volume Constraints

Recognizing that only constraining the minimum dose to the target and the maximum dose to the healthy structures would not result in an optimal treatment plan, Spirou *et al.* [6] was one of the first groups to introduce the dose-volume requirements into the radiation therapy

Structure Name	DVH Objective	Evaluator
PTV	D95%[cGy]	≥ 6650
Esophagus	V60Gy[%]	≤ 17
Heart	V50Gy[%]	≤ 25
Heart	V30Gy[%]	≤ 35
Heart	V5Gy[%]	≤ 50
Lungs-IGTV	V20Gy[%]	≤ 25
Lungs-IGTV	V25Gy[%]	≤ 20
Lungs-IGTV	V35Gy[%]	≤ 15
Lungs-IGTV	V50Gy[%]	≤ 10
Lungs-IGTV	V5Gy[%]	≤ 70

Table 1.1: The dose-volume requirements for a lung case.

treatment planning [7]. Nowadays, dose-volume-based constraints are an inseparable part of the optimization process in most commercial treatment planning systems.

Table 1.1 shows an example of the dose-volume requirements for a lung case. Let us look at the first constraint for the planning target volume (PTV). The PTV consists of the tumor plus a margin that surrounds it. We will provide a formal definition of the PTV in the following sections. The first constraint can be described as the following: at least 95% of the PTV should receive a dose greater than or equal to 6650 centigray (cGy). The second requirement, which constrains overdosing the esophagus, can be interpreted in the following way: no more than 17% of the esophagus should receive a dose greater than or equal to 60 gray (Gy). Furthermore, we can see the constraint on the mean dose to a healthy structure which limits the mean dose to the OAR to the prescribed dose.

The incorporation of the dose-volume constraints is one of the main challenges in radiation therapy treatment planning. In practice, each structure is discretized into small rectangular elements called voxels. There are a large number of voxels within each organ, making the treatment planning optimization problem large-scale in nature. Although dose-volume constraints play a crucial role in achieving high-quality treatment plans for patients, they induce non-convexity into the optimization problem, resulting in models that are computationally expensive to solve. In section 1.5, we will briefly discuss some of the models proposed to

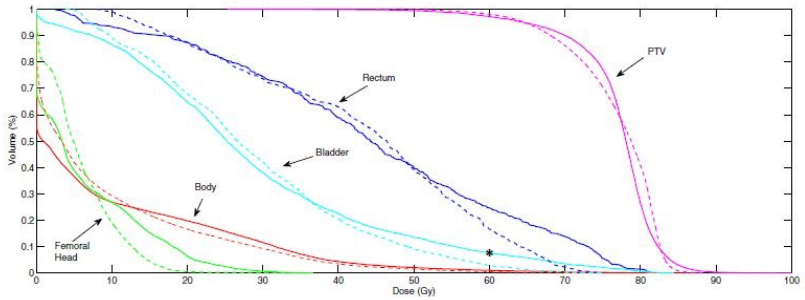

Figure 1.1: DVH for a prostate patient. The "*" denotes the point with coordinates $x = 60$ and $y = 0.1$ on the DVH of the bladder[1].

incorporate the dose-volume constraints in IMRT treatment planning.

1.4 Dose-Volume Histogram

There are two types of DVHs known as the differential DVH and the cumulative DVH. We will use the cumulative DVH for plan evaluation purposes in our study. The cumulative DVH, shown in Figure 1.1, is a non-increasing function. Each point on the cumulative DVH describes the percentage of the volume of the organ receiving dose greater than or equal to a specific amount. For instance, take the point with coordinates $x = 60$ and $y = 0.1$ on the DVH of the bladder for a prostate patient, which means that no more than 10% of the bladder receives a dose greater than or equal to 60 Gy. The DVH is one of the most common tools for evaluating a treatment plan after completing the optimization step.

1.5 Previous Work

Several models have been proposed to handle dose-volume constraints, including but not limited to mixed integer programming (MIP) and linear programming (LP) approaches. Langer *et al.* [8] presented a MIP approach to incorporate dose-volume requirements in radiation therapy treatment planning. In 2002, the MIP formulation was further investigated by Bednarz *et al.* [9]. Due to the large number of binary variables in the MIP formulation, these models are computationally expensive to solve. An LP approach was suggested by Romeijn *et al.* [10], where they further used the concept of conditional value-at-risk to bound the mean value of the tail of the differential DVH of a structure. Among other approaches proposed for handling the dose volume requirements, we can note the work of Spirou *et al.* [6], who used a gradient-based algorithm for this purpose. Zhang *et al.* [11] devised a greedy

approach, solving a sub-problem in each iteration. This method is time-consuming due to its trial-and-error nature.

The notion of generalized equivalent uniform dose (gEUD), also known as moments, was introduced to radiation therapy treatment planning by Niemierko *et al.* [12] as an alternative to purely DVH-based dose distribution. The incorporation of the gEUD into the treatment planning optimization problem was further investigated by Wu *et al.* [13], where the study involved the integration of the gEUD into the objective function. Comparing the resulting plans with those generated using dose-volume-based criteria, the authors' findings indicated that gEUD-based treatment plans could outperform the dose-volume-based plans in terms of sparing the healthy tissues. Building on the work of Wu *et al.*, Beong and Deasy [14] conducted further investigation into the utilization of the gEUD in radiation therapy treatment planning. Their study focused on analyzing the convexity of the gEUD equation when incorporated into either the objective function or constraints.

Zinchenko *et al.* [15] was the first group to propose using the gEUD values to approximate a desired DVH, highlighting the one-to-one correspondence between the DVH and an infinite sequence gEUD_α values for $\alpha = 1, 2, \ldots$. This approach showed promising results in terms of demanding less computing resources compared to the traditional dose-volume-based formulations. Following that, Zarepisheh *et al.* [1] proposed a convex-moment-based approach to replace the non-convex DVH constraints resulting in plans whose DVHs are close to the desired DVHs.

For more on dose-volume-based approaches, we refer the reader to Langer *et al.* [16], Wu *et al.* [17], Starkschall *et al.* [18] and Dai *et al.* [19].

1.6 Proton Therapy

Proton therapy is a type of external beam radiation therapy that uses protons to kill cancerous cells. There is an advantage to using protons to irradiate the tumor instead of traditional radiation such as X-ray. The X-rays have high energy when entering the body, irradiating healthy tissues on their way to the tumor. After reaching the tumor, they penetrate it with

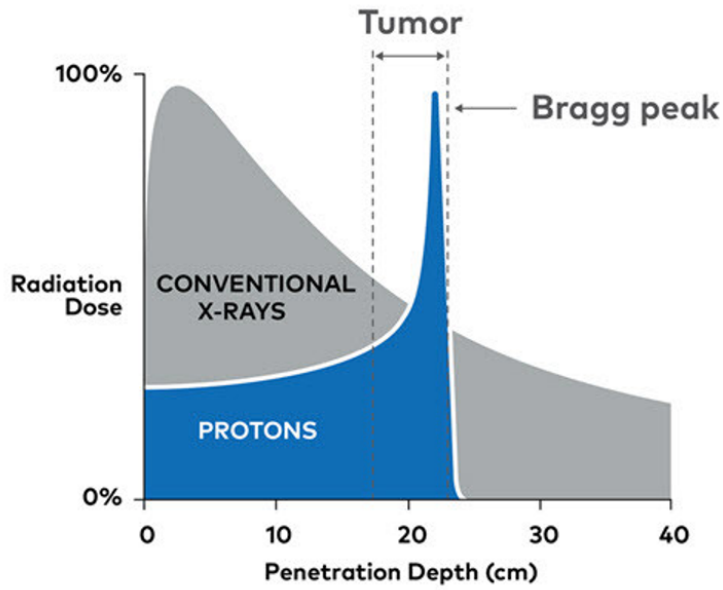

Figure 1.2: Dose distribution of protons versus x-rays [2].

high energy and exit the body.

Although their energy decreases as they travel through the body, they cause a lot of damage to the healthy tissues on their way. In contrast, protons have low energy when entering the body and have the ability to stop at the tumor, releasing their maximum energy, known as the Bragg peak, at the target, as shown in Figure 1.2. Therefore, proton therapy performs better at delivering a sufficient dose to the target while sparing the healthy tissues in the body.

Figure 1.3 illustrates the color wash dose distributions for a patient with lung cancer treated with photon and proton beams. The color scale on the right-hand side shows the dose intensity, where lower doses correspond to blue hues and higher doses to red hues. The figures distinctly showcase the differences in the behavior of proton and photon beams upon penetrating the patient's body, as described earlier.

1.7 Sources of Uncertainty in Radiation Therapy

Radiation therapy treatment planning is subject to a range of uncertainties that may arise either within a single treatment session or between sessions. These uncertainties can be

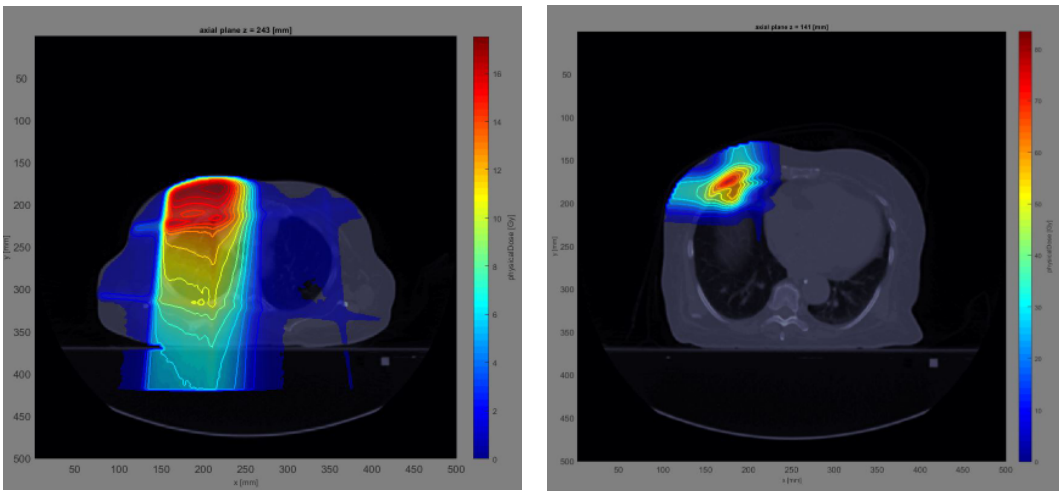

(a) Photon (b) Proton

Figure 1.3: The color wash dose distributions for a patient with lung cancer treated with photon and proton beams.

caused by factors such as patient movement or organ motion from breathing within one treatment session, or changes in the patient's weight and set-up errors from one treatment session to another. Disregarding the uncertainty in the treatment plan results in an uneven dose distribution, causing cold spots in the tumor.

A conventional method for addressing these uncertainties is to introduce a margin to the gross tumor volume (GTV), treating the area with a highly uniform dose. The GTV refers to the tumor itself. The clinical target volume (CTV) encompasses the GTV along with an additional margin to account for sub-clinical disease spread. The PTV, which includes the CTV plus a margin, accounts for uncertainties in planning or treatment delivery. Irradiating the PTV with a uniform dose produces a plan that is more robust against uncertainties. However, this approach can lead to increased radiation exposure to surrounding healthy structures, negatively impacting the patient's quality of life.

There have been numerous attempts to systematically create a robust treatment plan capable of addressing the uncertainties present during the course of treatment. One such approach relies on robust optimization, a sub-field of optimization that deals with uncertainties in the data. The assumption in the robust optimization is that the input data for the optimization problem is not precisely known but rather belongs to a set referred to as

the uncertainty set. By ensuring that the coefficients fall within this set, robust optimization guarantees that the constraints of the optimization problem at hand will not be violated. For an excellent reference on robust optimization, see [20].

Regarding the utilization of robust optimization in radiation therapy treatment planning, we can mention the work of Chu *et al.* [21] and Chan *et al.* [22]. Chu *et al.* have proposed a probabilistic method and a robust linear programming approach with ellipsoidal uncertainty set on the cumulative dose to a voxel for intensity-modulated radiation therapy. Chan *et al.* have developed a robust framework for handling uncertainties in breathing motion which outperforms the conventional methods of using margins around the tumor at sparing the healthy tissues.

In addition to photon therapy, robust optimization has also been employed in proton therapy treatment planning. The minimax approach, also known as the worst-case approach, has been utilized in IMPT. In this approach, the penalty associated with the worst-case scenario is minimized with the goal of obtaining a treatment plan that is as good as possible for the worst scenario. Unkelbach *et al.* ([23], [24]) have proposed a stochastic programming approach where each error scenario (for instance an overshoot or undershoot scenario caused by range uncertainty) is associated with an importance weight. This method involves assigning a high weight to probable scenarios while allocating a small weight to error scenarios that are considered feasible but improbable and minimizing the weighted sum of objective functions evaluated for all these error scenarios. For more on robust optimization in radiation therapy treatment planning, we refer the interested reader to [25].

1.8 Our Work

We will formulate and compare two optimization approaches for the treatment planning optimization problem in proton therapy focusing on a patient with lung cancer. We will first investigate a linear programming approach where we constrain the average dose to the healthy structures while ensuring that the target receives a sufficient dose. Subsequently, we will explore a moment-based approach built on the aforementioned linear programming model, where we incorporate a relaxation of the dose-volume requirements. Our goal is

to compare these models in terms of generating a good initial plan. We believe better basic models would result in more optimal final treatment plans. The models developed in this study are suitable for integration into the robust proton therapy treatment planning framework.

In Chapter 2, we will introduce the technical basics relevant to our work and describe the two optimization models in detail. In Chapter 3, we will discuss the experiments and how the input data was obtained using a radiation therapy treatment planning software named matRad. In Chapter 4, we will report the results and compare the two models in terms of both dosimetric outcomes and computational run-time, and in the final chapter, we will discuss future work.

Chapter 2

Methodology

2.1 Preliminaries

We begin by introducing some of the technical preliminaries relevant to our work.

2.1.1 Notation and Technical Basics

Deterministic quantities are represented using small case letters such as t and α, while deterministic vectors are represented using small case bold letters like $\mathbf{d}$ and $\mathbf{w}$. We use capital letters and their combinations, like F, DVH, and D, to denote functions and random variables. Matrices are represented using bold capital letters like $\mathbf{\Delta}$, and sets are represented using script capital letters such as $\mathcal{V}$.

As mentioned in the previous chapter, each treatment volume, including the target and the OARs, is discretized into small cubes known as voxels. For each structure with the voxel set $\mathcal{V}$ and the number of voxels equal to $|\mathcal{V}|$, let the vector $\mathbf{d} \in \Re^{|\mathcal{V}|}$ denote the dose to each voxel within the structure. Let the vector $\mathbf{w} \in \Re^{|\mathcal{B}|}$ determine the intensity of each beamlet, where $\mathcal{B}$ is the set of all beamlet indices of cardinality $|\mathcal{B}|$. Suppose $\mathbf{\Delta}_{v,b}$ represents the amount of dose that is delivered to voxel v at the unit intensity of beamlet b, then the dose

delivered to voxel v is

$$\mathbf{d}_v = \sum_{b \in \mathcal{B}} \mathbf{\Delta}_{v,b} \mathbf{w}_b. \tag{2.1}$$

The matrix $\mathbf{\Delta} \in \Re^{|\mathcal{V}| \times |\mathcal{B}|}$ with entries $\mathbf{\Delta}_{v,b}$ is known as the deposition matrix or the dose-influence matrix. With the deposition matrix fixed, we describe all realizable dose vectors with the following linear system of equations and inequalities,

$$\begin{cases} \mathbf{d} = \mathbf{\Delta} \mathbf{w}, \\ \mathbf{w} \geq 0. \end{cases} \tag{2.2}$$

For a structure with number of voxels equal to $|\mathcal{V}|$, the gEUD value for parameter α is defined as,

$$\text{gEUD}_\alpha = \left(\frac{1}{|\mathcal{V}|} \sum_{v \in \mathcal{V}} \mathbf{d}_v^\alpha \right)^{\frac{1}{\alpha}}. \tag{2.3}$$

where $\mathbf{d}_v$ denotes the dose to voxel v. The convexity of gEUD for $\alpha \geq 0$, with respect to the dose $\mathbf{d} \geq 0$, can be easily seen since it is a scalar multiple of the α-norm of the vector $\mathbf{d} \in \Re^{|\mathcal{V}|}$.

The α-degree moment of the dose delivered to a structure is defined as,

$$M_\alpha(\mathbf{d}) = \frac{1}{|\mathcal{V}|} \sum_{v \in \mathcal{V}} \mathbf{d}_v^\alpha. \tag{2.4}$$

2.1.2 A Simple Model

For better understanding, let us formulate a prototypical treatment planning optimization model without the incorporation of the dose-volume requirements. For simplicity, assume that we have only one target and one OAR with voxel indices $\mathcal{T}$ and $\mathcal{C}$ respectively. Let $\mathbf{d}_\mathcal{C}$ and $\mathbf{\Delta}_\mathcal{C}$ denote the dose vector and the dose-influence matrix for the healthy structure. Similarly, we define $\mathbf{d}_\mathcal{T}$ and $\mathbf{\Delta}_\mathcal{T}$ as the dose vector and the dose-influence matrix for the tumor. As there is a high chance that at least a few voxels in the target cannot meet the

prescribed homogeneous dose, a common approach is to relax this requirement by defining non-negative auxiliary variables $\mathbf{u}_t$ and $\mathbf{o}_t$ which quantify the degree to which the target is under- or over-dosed, respectively. By minimizing these variables in the objective function we are constraining the dose to each voxel of the target to remain between the minimum and maximum prescribed dose values.

The resulting model can be formulated in the following way:

$$\begin{aligned} \min_{\mathbf{w},\mathbf{d},\mathbf{o},\mathbf{u}} \quad & \sum_{c\in\mathcal{C}} \mathbf{d}_c + \sum_{t\in\mathcal{T}} (\mathbf{o}_t + \mathbf{u}_t) \\ \text{subject to} \quad & \mathbf{d}_{\mathcal{C}} = \mathbf{\Delta}_{\mathcal{C}}\mathbf{w}, \\ & \mathbf{d}_{\mathcal{T}} = \mathbf{\Delta}_{\mathcal{T}}\mathbf{w}, \\ & \mathbf{d}_t - \mathbf{o}_t \leq \pi_{max}, \qquad \forall t \in \mathcal{T}, \\ & \mathbf{d}_t + \mathbf{u}_t \geq \pi_{min}, \qquad \forall t \in \mathcal{T}, \\ & \mathbf{w}, \mathbf{o}, \mathbf{u} \geq 0, \end{aligned} \tag{2.5}$$

where constants π_{min} and π_{max} correspond to the minimum and maximum prescribed dose to the target, respectively.

2.2 Models Under Consideration

In this section, we will present the two models used in this study. For simplicity, we assume to have only one target and one healthy structure when describing the models. For our numerical experiments, we will extend the models to account for more than one OAR.

2.2.1 Linear Programming Approach

The LP formulation utilized in this study serves as a base model upon which the moment-based approach is constructed. Specifically, this model imposes constraints on the mean dose delivered to each healthy structure to its prescribed dose values. For the target, a similar approach as outlined in the prototype model (2.5) is adopted, whereby the under- and over-dose variables are minimized in the objective function to ensure that the dose to the target falls within the prescribed dose range.

The LP model is formulated as follows:

$$
\begin{aligned}
\min_{\mathbf{w},\mathbf{o},\mathbf{u}} \quad & \sum_{t\in\mathcal{T}} (\mathbf{o}_t + \mathbf{u}_t) \\
\text{subject to} \quad & \mathbf{d}_{\mathcal{C}} = \mathbf{\Delta}_{\mathcal{C}}\mathbf{w}, \\
& \mathbf{d}_{\mathcal{T}} = \mathbf{\Delta}_{\mathcal{T}}\mathbf{w}, \\
& \tfrac{1}{|\mathcal{C}|}\sum_{c\in\mathcal{C}} \mathbf{d}_c \leq \tau_{mean}, \\
& \mathbf{d}_t - \mathbf{o}_t \leq \pi_{max}, \qquad \forall t \in \mathcal{T}, \\
& \mathbf{d}_t + \mathbf{u}_t \geq \pi_{min}, \qquad \forall t \in \mathcal{T}, \\
& \mathbf{w}, \mathbf{o}, \mathbf{u} \geq 0,
\end{aligned}
\tag{2.6}
$$

where constants π_{min} and π_{max} correspond to the minimum and maximum prescribed dose to the target, and τ_{mean} refers to the mean prescribed dose to the healthy structure, respectively.

2.2.2 Moment-Based Approach

The formal relationship between the gEUD values and the DVH was investigated in [15]. Zinchenko *et al.* [15] note: "Given a DVH, the infinite sequence of values $\left\{\text{gEUD}_\alpha\right\}_{\alpha=1,2,\ldots}$ is determined uniquely. Conversly, the sequence $\left\{\text{gEUD}_1, \text{gEUD}_2, \text{gEUD}_3, \ldots\right\}$ uniquely determines the DVH." Drawing from this fact, Zarepisheh *et al.* [1] proposed a moment-based approach, which we will adopt in this study.

Let $\bar{\mathbf{d}}$ denote some ideal, not necessarily realizable, dose corresponding to the reference DVH. For a given structure, the reference DVH refers to a dose-volume histogram meeting all the prescribed dose-volume criteria.

We define the reference moments as,

$$
\begin{aligned}
\mu_\alpha^{\mathcal{C}} &= M_\alpha\left(\bar{\mathbf{d}}_{\mathcal{C}}\right), \\
\mu_\omega^{\mathcal{T}} &= M_\omega\left(\bar{\mathbf{d}}_{\mathcal{T}}\right).
\end{aligned}
\tag{2.7}
$$

To obtain the reference moments, it is not required to know $\bar{\mathbf{d}}$ explicitly. The differential DVH, denoted as DVH_Δ, can be used to calculate the first reference moment as follows:

$$\mu_1^{\mathcal{C}} = \int_0^\infty t\ \mathrm{DVH}_\Delta(t)\,dt = -t\ \mathrm{DVH}(t)|_0^\infty + \int_0^\infty \mathrm{DVH}(t)\,dt = \int_0^\infty \mathrm{DVH}(t)\,dt. \tag{2.8}$$

Note that in $M\int_0^\infty \mathrm{DVH}(t)dt$, we can replace the upper integration limit $+\infty$ with $\delta_{\max}$, which represents the highest dose allowed to the structure. The higher degree reference moments for the OARs and the target are calculated in a similar way.

To achieve a treatment plan resulting in a dose distribution that matches the reference DVHs, it suffices to solve the following semi-infinite non-linear feasibility problem,

$$\begin{cases} \mathbf{d}_{\mathcal{C}} = \mathbf{\Delta}_{\mathcal{C}}\mathbf{w}, \\ \mathbf{d}_{\mathcal{T}} = \mathbf{\Delta}_{\mathcal{T}}\mathbf{w}, \\ M_\alpha(\mathbf{d}_{\mathcal{C}}) = \mu_\alpha^{\mathcal{C}}, \quad \alpha = 1,\ldots,\infty, \\ M_\omega(\mathbf{d}_{\mathcal{T}}) = \mu_\omega^{\mathcal{T}}, \quad \omega = 1,\ldots,\infty, \\ \mathbf{w} \geq 0, \end{cases} \tag{2.9}$$

where the moments are defined as in (2.4), and $\mu_\alpha^{\mathcal{T}}, \mu_\omega^{\mathcal{T}}$ correspond to the reference moments, defined as in (2.7), for the OAR and target respectively.

There are two main challenges in solving the problem (2.9).

The moment constraints specified in (2.7) are non-convex. Although the moments are convex and increasing functions of the dose, the equalities in the constraint specification result in non-convex constraints. To address this, we replace the equality constraints,

$$M_\alpha(\mathbf{d}_{\mathcal{C}}) = \mu_\alpha^{\mathcal{C}}, \quad \alpha = 1,\ldots,\infty \tag{2.10}$$

by the inequality constraints

$$M_\alpha(\mathbf{d}_{\mathcal{C}}) \leq \mu_\alpha^{\mathcal{C}}, \quad \alpha = 1,\ldots,\infty. \tag{2.11}$$

Furthermore, the problem has an infinite number of constraints. To overcome this issue, we use a finite number of moment constraints (first and second-degree moments) for each structure.

Keeping this in consideration, the moment-based approach is formulated in the following way:

$$
\begin{aligned}
\min_{\mathbf{w},\mathbf{o},\mathbf{u}} \quad & \sum_{t\in\mathcal{T}} (\mathbf{o}_t + \mathbf{u}_t) \\
\text{subject to} \quad & \mathbf{d}_{\mathcal{C}} = \mathbf{\Delta}_{\mathcal{C}}\mathbf{w}, \\
& \mathbf{d}_{\mathcal{T}} = \mathbf{\Delta}_{\mathcal{T}}\mathbf{w}, \\
& M_\alpha(\mathbf{d}_{\mathcal{C}}) \le \mu_\alpha^{\mathcal{C}}, \qquad \alpha = 1, 2 \\
& \tfrac{1}{|\mathcal{C}|}\sum_{c\in\mathcal{C}} \mathbf{d}_c \le \tau_{mean}, \\
& \mathbf{d}_c \le \tau_{max}, \qquad \forall c \in \mathcal{C}, \\
& \mathbf{d}_t - \mathbf{o}_t \le \pi_{max}, \qquad \forall t \in \mathcal{T}, \\
& \mathbf{d}_t + \mathbf{u}_t \ge \pi_{min}, \qquad \forall t \in \mathcal{T}, \\
& \mathbf{w}, \mathbf{o}, \mathbf{u} \ge 0,
\end{aligned}
\tag{2.12}
$$

To keep our model simple, we have not used moment-based constraints for the target and used an approach similar to the methodology employed in (2.5) to avoid under- or over-dosing the target.

Chapter 3

Computational Set up and Results

3.1 Patient Data and Plan Objectives

To evaluate the performance of our models, we performed our study on a patient with lung cancer; for a sample geometry, see Figure 3.1. The anonymized patient data was provided by our collaborators at the University of Pennsylvania. It is worth noting that for this study, we have used the clinical data of a patient who has undergone prior treatment. To obtain the plan parameters suitable for this patient, we imported their CT scans into Eclipse [26]. Eclipse is a treatment planning system developed by Varian medical systems, which is used to create a treatment plan given the data of a patient. After importing the CT scans of our patient into Eclipse, we defined two beams at angles 0° and 270° based on the experience of the radiation oncologist. As the tumor for this patient is close to the surface of the body, we have introduced two range shifters (RS) with a width of 5 cm for each beam. A range shifter is a stopping material inserted between the nozzle and the patient, which is used to reduce the beam energy when the tumor is in a shallow depth [27]. We have introduced a margin of 1 cm around the tumor to ensure that the target receives a uniform dose and is sufficiently

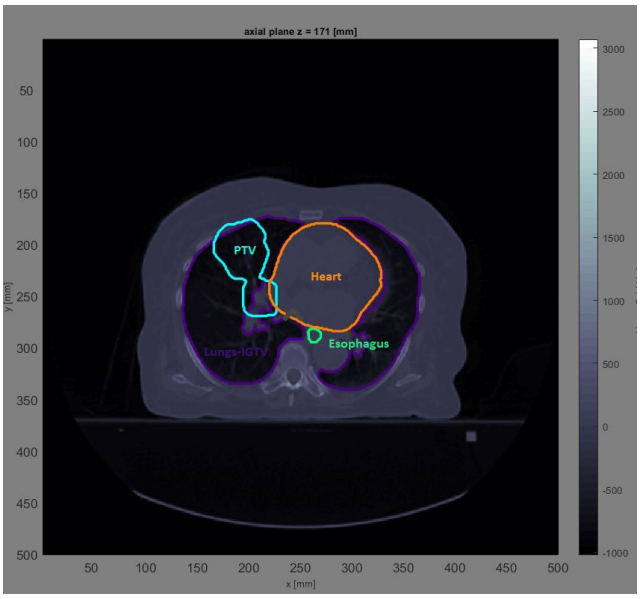

Figure 3.1: CT slice of the lung patient scan with contours for structures of interest.

irradiated. After defining the plan parameters, we initialized the optimization module of Eclipse to obtain the DVHs. Please note that multiple iterations of the optimization step may be necessary to yield a high-quality treatment plan. After achieving an acceptable plan, see Figure 3.2, we exported the CT files from Eclipse, now containing the plan parameters.

As mentioned earlier, to derive the dose vector for each structure, we need to calculate the dose-influence matrix specific to each organ. In this study, we have used matRad [28] to find the dose-influence matrices. matRad is an open-source software for radiation therapy treatment planning developed entirely in Matlab. The first step in obtaining the dose-influence matrices is to import the patient data into matRad. Using matRad's Digital Imaging and Communications in Medicine (DICOM) import module, we imported the CT data obtained from Eclipse, now containing the plan parameters, such as the width of the range shifter, into Matlab. This module can be accessed via the graphical user interface (GUI) or by calling the relevant function manually.

Once the files are imported, this module stores the data obtained from the DICOM files into a Matlab structure and cell array named ct and cst, respectively. The ct structure contains information about the voxels, such as their size and number in the x-, y-, and z- directions. The cell array cst contains information about the volumes of interest (VOI), including but not limited to the VOI's name, type (whether the VOI is an OAR, a target volume, or

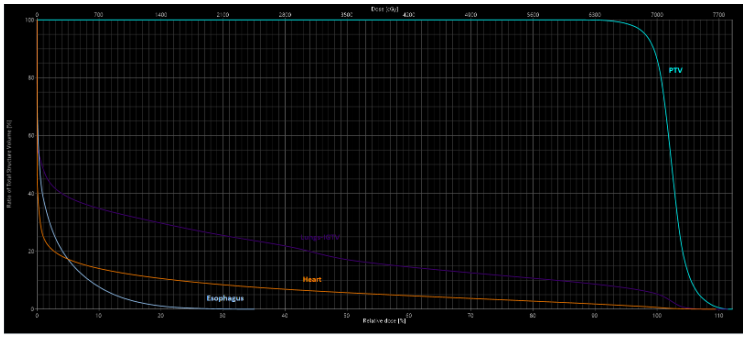

Figure 3.2: The DVHs exported from Eclipse.

should be ignored), and voxel indices (vectors containing the indices of all voxels covered by the VOI) [29]. The next step is to determine the treatment plan parameters, which can be accomplished in two ways: via the GUI or using the Matlab structure named pln. The plan parameters to be specified are the radiation modality (photons, protons, and carbon), gantry and couch angles, the iso-center, the number of fractions, and the voxel width. Following that, the dose calculation function can be called in the same two ways mentioned earlier. Within matRad, the conventional dose-to-water-pencil beam algorithm described in [30] is employed to compute the dose deposition matrix for the proton module [31]. The dose calculation function returns the structure dij, which holds the dose-influence matrix stored in a cell named physicalDose. The size of the dose-influence matrix generated by matRad is $|\mathcal{V}| \times |\mathcal{B}|$, where $|\mathcal{V}|$ represents the number of voxels in all the structures, and $|\mathcal{B}|$ denotes the number of beams. The resulting matrix was used as the input to both our moment and LP approaches. It is worth noting that matRad has a built-in optimization algorithm that relies on the interior point optimizer package (IPOPT) [32] to solve the treatment planning optimization problem given a set of clinical objectives [31]. Upon solving the optimization problem, matRad generates the DVHs for each organ. In our study, however, we have only used the dose-influence matrices generated by matRad and implemented our own optimization models.

Regarding the beam arrangements, we used two fields at the gantry angles $0°$ and $270°$, which have been pre-defined when developing a plan in Eclipse. We used the proton radiation mode with 3 mm voxel width. The number of fractions was used at its default value of 30, and the iso-center was determined through calculations performed by matRad. This resulted in a total of $120,182$ voxels for three OARs and $7,599$ for the target and a total of $83,359$

Structure Name	DVH Objective	Evaluator
Esophagus	Mean[cGy]	≤ 3400
Heart	Mean[cGy]	≤ 1000
Lungs-IGTV	Mean[cGy]	≤ 1800

Table 3.1: The mean dose constraints for the OARs.

beamlets.

The planning objectives for this patient consist of a minimum prescribed dose of 70 Gy and a maximum prescribed dose of 72 Gy to the PTV for both the LP and moment-based approach. For the LP approach, we constrain the mean dose to the healthy structures as in Table 3.1. For the moment-based approach, in addition to limiting the mean dose to each structure, we add second-moment constraints as in (2.12), corresponding to the dose-volume requirements as specified in Table 3.2. Furthermore, we limit the maximum dose to each healthy structure to 72 Gy.

In particular, the moment-based approach requires calculating the reference moments. These reference moments can be obtained from the reference DVHs. One strategy for finding the reference DVHs is to utilize the treatment plans from patients who were previously treated and had the same type and stage of cancer. This method requires having a database containing treatment plans of previously treated patients in addition to an algorithm capable of identifying the best match based on the location of the tumor and the organs involved.

An alternative methodology is to create the reference DVHs based on the dose-volume requirements prescribed for the specific patient. Given a set of critical points, one can construct a reference DVH by connecting these points forming a piece-wise linear function.

In this study, we have used the second approach, constructing the reference DVHs from the patient's prescribed dose requirements provided by the University of Pennsylvania. Figure 3.3 shows the reference DVHs for the OARs created by connecting the critical DVH points

Structure Name	DVH Objective	Evaluator	Acceptable Variation
Esophagus	Mean[cGy]	≤ 3400	-
Heart	V50Gy[%]	≤ 25	-
Heart	V30Gy[%]	≤ 35	-
Heart	V5Gy[%]	≤ 50	-
Heart	Mean[cGy]	≤ 1000	2000
Lungs-IGTV	V20Gy[%]	≤ 25	35
Lungs-IGTV	V25Gy[%]	≤ 20	30
Lungs-IGTV	V35Gy[%]	≤ 15	25
Lungs-IGTV	V50Gy[%]	≤ 10	20
Lungs-IGTV	V5Gy[%]	≤ 70	75
Lungs-IGTV	Mean[cGy]	≤ 1800	2000

Table 3.2: The dose-volume requirements for the OARs.

based on the dose-volume constraints outlined in Table 3.2.

3.2 Computational Environment

The computational experiments were conducted on a workstation equipped with AMD Ryzen 7 4800H with eight 2.90 GHz cores and 16 GB RAM. Both the linear and the moment-based approaches were implemented in Matlab R2021a with CVX using Gurobi v9.00. CVX is a modeling system for building and solving disciplined convex programming problems, which supports several standard problem types, including linear and quadratic, second-order cone, and semi-definite programs.

3.3 Model Evaluation Criteria

Our primary objective is to evaluate both the LP and moment-based models in terms of generating a good initial plan which can be further enhanced with an emphasis on the controllability of the resulting DVHs. For this purpose, we will compare the two models with regard to:

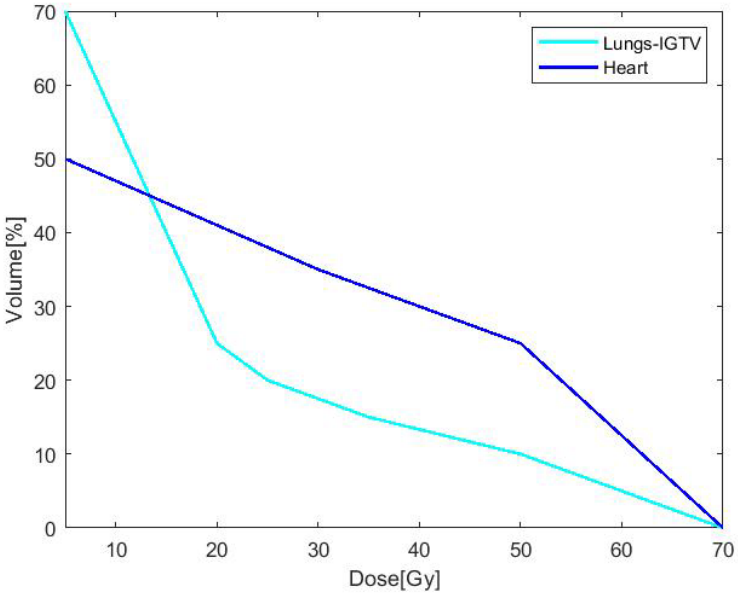

Figure 3.3: The reference DVHs used for the lung patient.

- generating an initial treatment plan of good quality,
- producing the plan in a time-frame suitable for clinical use, utilizing conventional computing resources.

3.4 Numerical Results

3.4.1 The Linear Programming Approach

We first start by presenting the results of the LP approach. As mentioned earlier, in this approach, we are constraining the mean dose to the healthy structures without incorporating the dose-volume requirements. For the target, we are penalizing over- or under-dosing the PTV. In Figure 3.4, we can see the resulting DVHs. For the PTV, at least 95.8% of the volume receives the prescribed dose of 70 Gy, while 6.7% of the volume receives a dose greater than 72 Gy. The minimum dose to the PTV is 69 Gy, and the maximum dose is 73 Gy. For the OARs, the mean dose to the lungs-IGTV, heart, and esophagus is 18.8, 10, and 34 Gy respectively, satisfying the mean dose constraints for the heart and the esophagus and meeting the acceptable variation for the lungs-IGTV. The run-time for the LP approach is approximately 1.5 hour.

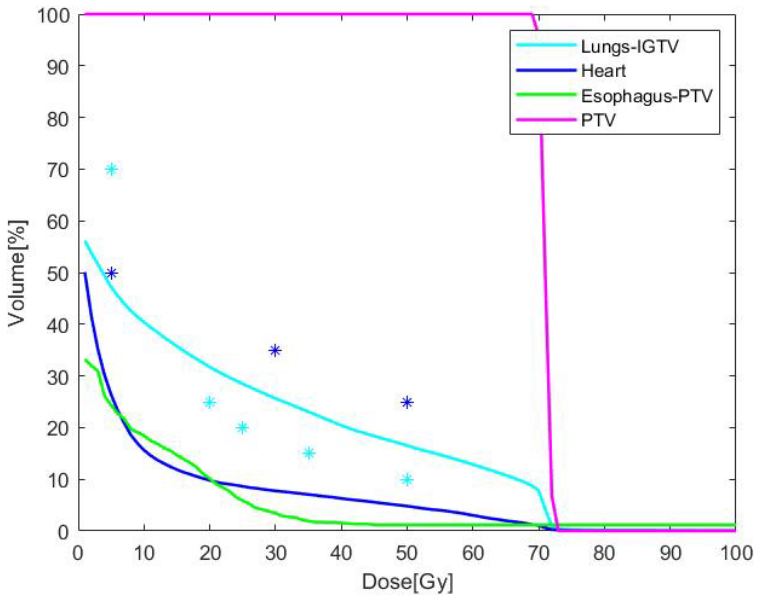

Figure 3.4: The resulting DVHs for the LP approach, where the "*" represents the critical DVH points.

3.4.2 The Moment-based Approach

In this approach, we are implementing the dose-volume requirements on top of the linear model, in other words imposing more limitations on the dose delivered to the healthy structures. We use the same method as in the LP approach for the target.

In our first experiment running the moment-based model, the program terminated unexpectedly due to memory overflow. Therefore, we investigated the dose influence matrices for each structure to find the underlying factors. The deposition matrices in the treatment planning optimization problem are highly sparse. We observed that the dose-influence matrices for the lungs-IGTV, heart, esophagus, and PTV contain approximately 1.3%, 0.13%, 0.9%, and 1.8% non-zero values, respectively. The total number of non-zeros in these matrices is $118,899,327$. Moreover, our investigation revealed that the values in the dose-influence matrices range from as small as $1.2852e-21$ to $2.0695e-05$ for the OARs and $8.3957e-21$ to $9.4484e-06$ for the target for this patient.

The Gurobi optimizer offers two primary methods for solving continuous models and the continuous relaxations of MIP models: the barrier and the simplex algorithm. For our

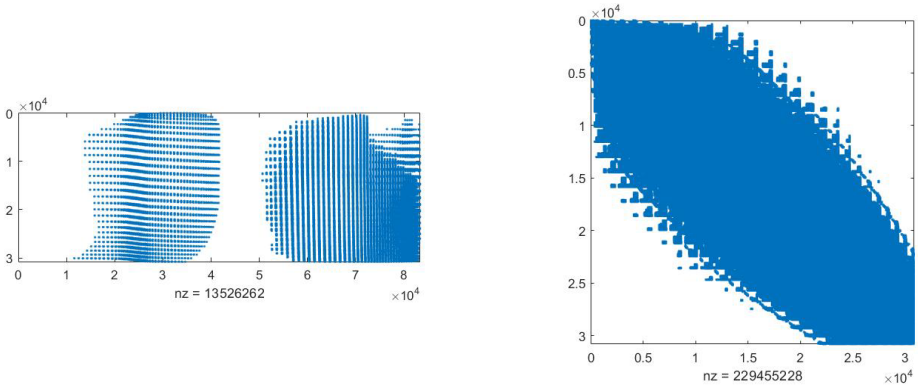

(a) A (b) AA^T

Figure 3.5: The sparsity patterns of matrices A and AA^T.

model, which is a second-order conic programming (SOCP) problem, Gurobi uses the barrier algorithm. It is worth mentioning that generally, the barrier algorithm performs better for complex, large-scale models; however, it is more numerically sensitive [33].

In each iteration of the barrier algorithm, the scaled matrix AA^T is formed, and subsequently, Cholesky factorization is performed. Here, matrix A corresponds to the dose influence matrix for each structure. Figure 3.5, shows the sparsity patterns of matrices A and AA^T. We can observe that matrix A has $13,526,262$ non-zeros and this number increases to $229,455,228$ in AA^T. Furthermore, the Cholesky factor L, where $A = LL^T$, contains more non-zeros compared to A, as the computation of the Cholesky factorization creates fill-in non-zeros. Therefore, storing the matrix AA^T and performing the factorization operations for a matrix with a large number of non-zeros within a small range would require significant memory resources.

To reduce the memory requirements, we decided to experiment with several variants of sparsification strategies. As previously noted, each entry of the dose influence matrix determines the amount of dose that each voxel receives. It is worth noting that a subset of these entries which have small values, capture scattered energy. Therefore, converting small values to zero does not affect the overall quality of the treatment plan.

In our first experiment, we used an aggressive sparsification method, converting any number less than 10^{-5} and 10^{-7} to 0 for the OARs and the PTV, respectively, resulting in the total

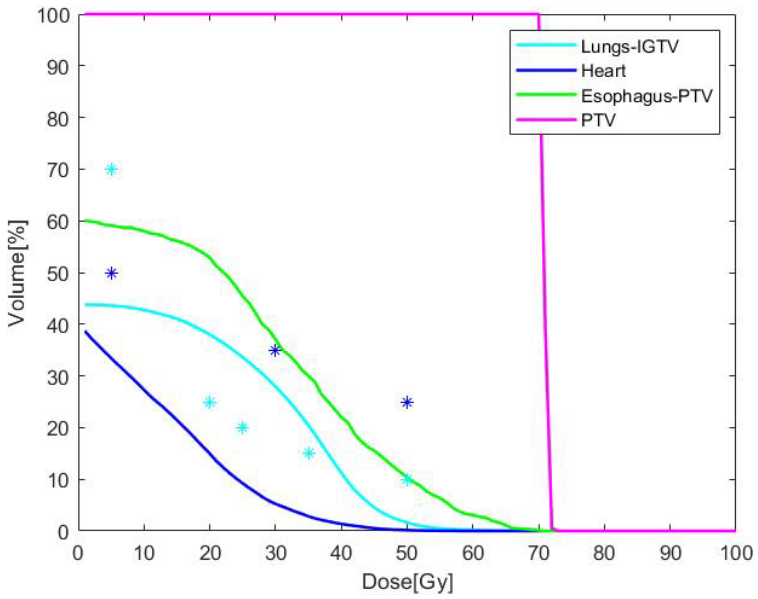

Figure 3.6: The resulting DVHs for Method 1, where the "*" represents the critical DVH points.

number of 13, 699, 756 non-zeros in the deposition matrices. See Figure 3.6 for the resulting DVHs. Henceforth, we will refer to the this approach as Method 1. The minimum dose to the PTV is 70 Gy, and the maximum dose is 72 Gy. For the OARs, the mean dose to the lungs-IGTV, heart, and esophagus is 14.37, 6.8, and 21.32 Gy respectively, satisfying all the mean dose constraints. The maximum dose to the lungs-IGTV, heart, and esophagus is 70.34, 59.65, and 70.91 Gy respectively, not exceeding the maximum prescribed dose for any of the healthy structures. In terms of the dose volume requirements for the lungs-IGTV and the heart, see Table 3.3. From the table, we can see that Method 1 has met all the requirements for the heart while has been able to meet two requirements and one acceptable variation for the lungs-IGTV. The run-time for this approach is approximately 3 minutes.

In our next experiment, we used a less aggressive sparsification method, converting any number less than 0.6×10^{-5} and 10^{-7} to 0 for the OARs and the PTV respectively, resulting in the total number of 22, 816, 928 non-zeros in the deposition matrices. See Figure 3.7 for the resulting DVHs. Henceforth, we will refer to this approach as Method 2. For the PTV, the results are the same as the previous moment-based approach. For the OARs, the mean dose to the lungs-IGTV, heart, and esophagus is 17.52, 8.87, and 33.91 Gy respectively, satisfying all the mean dose constraints. The maximum dose to the lungs-IGTV, heart, and

Structure Name	Dose (Gy)	Volume (%)	Meeting the Requirement
Heart	5	33	✓
Heart	30	5	✓
Heart	50	0	✓
Lungs-IGTV	5	44	✓
Lungs-IGTV	20	38	✗
Lungs-IGTV	25	34	✗
Lungs-IGTV	35	20	✻
Lungs-IGTV	50	2	✓

Table 3.3: Shows whether the dose-volume requirement has been met in Method 1. "✓" identifies as meeting and "✗" identifies as not meeting the requirement, and "✻" identifies as meeting the acceptable variation.

esophagus is 71.94, 48.19, and 70.77 Gy respectively, not exceeding the maximum prescribed dose for any of the healthy structures. In terms of the dose volume requirements for the lungs-IGTV and the heart, see Table 3.4. From the table, we can see that Method 2 has met all the requirements for the heart while has been able to meet two requirements and one acceptable variation for the lungs-IGTV. The run-time for this approach is approximately 34 hours.

In our final experiment, we set all values less than 10^{-7} to 0 for the OARs and the PTV resulting in the total number of $98,428,835$ non-zeros in the deposition matrices. Running this model on a machine with 16 GB of memory was infeasible due to memory constraints. As a result, we attempted to run the model on a machine with 143 GB of memory. However, after running the program for a week, we manually terminated it as the model was deemed unsuitable for clinical use. The results obtained by the one-week mark were inconclusive.

In the next section, we will summarize the results of our experiments in terms of both the dosimetric outcomes and computational run-time.

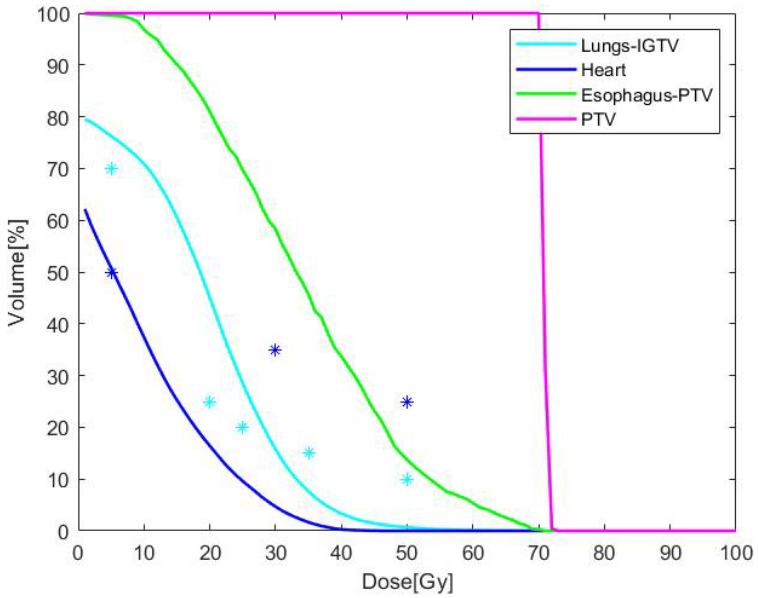

Figure 3.7: The resulting DVHs for Method 2, where the "*" presents the critical DVH points.

Structure Name	Dose (Gy)	Volume (%)	Meeting the Requirement
Heart	5	50	✓
Heart	30	5	✓
Heart	50	0	✓
Lungs-IGTV	5	76	✗
Lungs-IGTV	20	45	✗
Lungs-IGTV	25	29	✻
Lungs-IGTV	35	8	✓
Lungs-IGTV	50	1	✓

Table 3.4: Shows whether the dose-volume requirement has been met for Method 2. "✓" identifies as meeting and "✗" identifies as not meeting the requirement, and "✻" identifies as meeting the acceptable variation.

3.5 Comparative Results

3.5.1 Dosimetric Outcome

In terms of PTV coverage, the moment-based approach outperforms the LP approach, satisfying the minimum/maximum dose requirements. In the moment-based approach, the PTV receives at least 70 Gy and at most 72 Gy, while in the LP approach, at most 4.2% of the PTV receives a dose less than 70 Gy and approximately 6% of the volume, receives a dose greater than 72 Gy. Despite using the same constraints and objective function for the target in both the LP and moment-based approaches, we have observed different results. This outcome can be attributed to the sparsification of dose deposition matrices for the moment-based approach, which leads to a considerably smaller model and different results. For the PTV, both Method 1 and Method 2 for the moment-based approach yield the same result.

Regarding the OARs, the moment-based approach provides better results as we are imposing more restrictions on the dose requirements for the lungs-IGTV and the heart. It is worth noting that in the moment-based approach, we are not implementing dose-volume requirements for the esophagus, and we are only limiting the mean dose.

Comparing the two sparsification methods used in the moment-based approach, in terms of dose-volume requirements for the healthy structures, we see that in both approaches, the dose-volume requirements for the heart have been satisfied. For the lungs-IGTV, both Method 1 and Method 2 satisfied two requirements and one acceptable variation. It is important to note that in Method 2, for the lungs-IGTV, as the dose increases, the relative volume decreases, meaning that the OARs receive less dose in Method 2 compared to Method 1. For instance, in the second method for the lungs-IGTV, approximately 8% of the volume receives 35 Gy, while in the first approach, approximately 20% of the volume receives 35 Gy.

3.5.2 Computational Run-time

As we observed, the moment-based approach Method 1 has the fastest run-time of approximately 3 minutes, followed by the LP approach at 1.5 hour, and then the moment-based

approach Method 2 at 34 hours. The moment-based approach Method 1 is the only method suitable for clinical use in terms of computational run-time. Although the moment-based approach is a more sophisticated model with second-order conic constraints, Method 1 has a faster run-time compared to the LP approach. This finding could be explained due to faster computations for sparse problems, as opposed to problems of comparable size but higher density.

Chapter 4

Conclusion and Future Work

4.1 Conclusion

In this study, we have formulated and implemented two approaches for proton therapy treatment planning optimization problem, namely the linear programming and the moment-based approach. We assessed these models based on their ability to generate good-quality initial treatment plans, as we assume that better initial plans would lead to higher-quality final plans. We compared these models in terms of dosimetric outcomes and computational run-time. It is noteworthy that we performed this study on the clinical data of a patient with lung cancer.

For the target, we penalized over- and under-dosing the PTV in both approaches. In the LP approach, we constrained the mean dose to the healthy structures, while in the moment-based approach, we went one step further, incorporating the dose-volume requirements into the treatment planning optimization problem. We observed that the moment-based approach outperforms the LP model in terms of target coverage. Regarding the OARs, as expected, the moment-based approach yields better results compared to the LP approach as we are imposing more limitations on the dose delivered to the healthy structures. However, as the model becomes more sophisticated, there will be additional drawbacks to consider,

in this case, higher memory usage and slower computational run-time.

Due to the high memory usage required for solving the moment-based approach, we offered a solution setting all values less than a specific threshold to 0 in the dose deposition matrices for the target and the OARs. First, we used an aggressive sparsification method reducing the number of non-zero elements from $118,899,327$ to $13,699,756$. Although this approach satisfied all the dose-volume requirements for the heart, it violated two requirements for the lungs-IGTV with a run-time of approximately 3 minutes, which is considered suitable for clinical implementation.

Subsequently, we used a less aggressive sparsification method this time, reducing the number of non-zero elements from $118,899,327$ to $22,816,928$. This approach satisfied all the dose-volume constraints for the heart and violating two requirements for the lungs-IGTV. Moreover, Method 2 led to better dosimetric outcomes, outperforming the previous approach in sparing the healthy structures while providing the same coverage for the target. The run-time for this method was approximately 34 hours, which is considerably higher than the previous moment-based approach.

Therefore, we can conclude that there is a trade-off between the quality of the plan in terms of dosimetric outcomes and the computational run-time. As we use a less strict sparsification method in the moment-based approach, we anticipate achieving higher-quality treatment plans but at the expense of increased run-time.

4.2 Future Work

For future work we suggest investigating other sparsification methods for the moment-based approach to further optimize the trade-off between dosimetric outcomes and computational run-time. Further studies could also expand the scope of this work by evaluating the performance of the moment-based approach on larger patient datasets and other disease sites.

Furthermore, as mentioned earlier in Chapter 1, the moment-based approach formulated in this study is well-suited to be embedded into the robust proton therapy treatment planning

framework. Based on the type of cancer and source of uncertainty, the moment-based approach can be combined with existing robust optimization models such as the work of Chu *et al.* [21] and Chan *et al.*[22]. This can lead to treatment plans that not only satisfy the dose-volume requirements but are also more robust against uncertainty, resulting in a higher quality of life for the patient.

References

[1] M. Zarepisheh, M. Shakourifar, G. Trigila, P. Ghomi, S. Couzens, A. Abebe, L. Noreña, W. Shang, S. B. Jiang, and Y. Zinchenko, "A moment-based approach for dvh-guided radiotherapy treatment plan optimization," *Physics in Medicine & Biology*, vol. 58, no. 6, p. 1869, 2013.

[2] V. M. Systems, "Benefits of intensity modulated proton therapy," 2023.

[3] C. C. Society, "Cancer statistics at a glance," 2023.

[4] C. C. Society, "Treatment types," 2023.

[5] C. C. Society, "Radiation therapy," 2023.

[6] S. V. Spirou and C.-S. Chui, "A gradient inverse planning algorithm with dose-volume constraints," *Medical physics*, vol. 25, no. 3, pp. 321–333, 1998.

[7] B. Cho, "Intensity-modulated radiation therapy: a review with a physics perspective," *Radiation oncology journal*, vol. 36, no. 1, p. 1, 2018.

[8] M. Langer, R. Brown, M. Urie, J. Leong, M. Stracher, and J. Shapiro, "Large scale optimization of beam weights under dose-volume restrictions," *International Journal*

of Radiation Oncology Biology* Physics*, vol. 18, no. 4, pp. 887–893, 1990.

[9] G. Bednarz, D. Michalski, C. Houser, M. S. Huq, Y. Xiao, P. R. Anne, and J. M. Galvin, "The use of mixed-integer programming for inverse treatment planning with pre-defined field segments," *Physics in Medicine & Biology*, vol. 47, no. 13, p. 2235, 2002.

[10] H. E. Romeijn, R. K. Ahuja, J. F. Dempsey, A. Kumar, and J. G. Li, "A novel linear programming approach to fluence map optimization for intensity modulated radiation therapy treatment planning," *Physics in Medicine & Biology*, vol. 48, no. 21, p. 3521, 2003.

[11] Y. Zhang and M. Merritt, "Dose-volume-based imrt fluence optimization: A fast least-squares approach with differentiability," *Linear Algebra and its Applications*, vol. 428, no. 5-6, pp. 1365–1387, 2008.

[12] A. Niemierko, "Reporting and analyzing dose distributions: a concept of equivalent uniform dose," *Medical physics*, vol. 24, no. 1, pp. 103–110, 1997.

[13] Q. Wu, R. Mohan, and A. Niemierko, "Imrt optimization based on the generalized equivalent uniform dose (eud)," in *Proceedings of the 22nd Annual International Conference of the IEEE Engineering in Medicine and Biology Society (Cat. No. 00CH37143)*, vol. 1, pp. 710–713, IEEE, 2000.

[14] B. Choi and J. O. Deasy, "The generalized equivalent uniform dose function as a basis for intensity-modulated treatment planning," *Physics in Medicine & Biology*, vol. 47, no. 20, p. 3579, 2002.

[15] Y. Zinchenko, T. Craig, H. Keller, T. Terlaky, and M. Sharpe, "Controlling the dose distribution with geud-type constraints within the convex radiotherapy optimization framework," *Physics in Medicine & Biology*, vol. 53, no. 12, p. 3231, 2008.

[16] M. Langer and J. Leong, "Optimization of beam weights under dose-volume restrictions," *International Journal of Radiation Oncology* Biology* Physics*, vol. 13, no. 8, pp. 1255–1260, 1987.

[17] Q. Wu and R. Mohan, "Algorithms and functionality of an intensity modulated radiotherapy optimization system," *Medical physics*, vol. 27, no. 4, pp. 701–711, 2000.

[18] G. Starkschall, A. Pollack, and C. W. Stevens, "Treatment planning using a dose–volume feasibility search algorithm," *International Journal of Radiation Oncology* Biology* Physics*, vol. 49, no. 5, pp. 1419–1427, 2001.

[19] J. Dai and Y. Zhu, "Conversion of dose–volume constraints to dose limits," *Physics in Medicine & Biology*, vol. 48, no. 23, p. 3927, 2003.

[20] A. Ben-Tal, L. El Ghaoui, and A. Nemirovski, *Robust optimization*, vol. 28. Princeton university press, 2009.

[21] M. Chu, Y. Zinchenko, S. G. Henderson, and M. B. Sharpe, "Robust optimization for intensity modulated radiation therapy treatment planning under uncertainty," *Physics in Medicine & Biology*, vol. 50, no. 23, p. 5463, 2005.

[22] T. C. Chan, T. Bortfeld, and J. N. Tsitsiklis, "A robust approach to imrt optimization," *Physics in Medicine & Biology*, vol. 51, no. 10, p. 2567, 2006.

[23] J. Unkelbach, T. C. Chan, and T. Bortfeld, "Accounting for range uncertainties in the optimization of intensity modulated proton therapy," *Physics in Medicine & Biology*, vol. 52, no. 10, p. 2755, 2007.

[24] J. Unkelbach, T. Bortfeld, B. C. Martin, and M. Soukup, "Reducing the sensitivity of impt treatment plans to setup errors and range uncertainties via probabilistic treatment planning," *Medical physics*, vol. 36, no. 1, pp. 149–163, 2009.

[25] J. Unkelbach, M. Alber, M. Bangert, R. Bokrantz, T. C. Chan, J. O. Deasy, A. Fredriksson, B. L. Gorissen, M. Van Herk, W. Liu, *et al.*, "Robust radiotherapy planning," *Physics in Medicine & Biology*, vol. 63, no. 22, p. 22TR02, 2018.

[26] V. M. Systems, "Eclipse," 2023.

[27] W. Matysiak, D. Yeung, R. Slopsema, and Z. Li, "Evaluation of the range shifter model for proton pencil-beam scanning for the eclipse v. 11 treatment planning system," *Journal of Applied Clinical Medical Physics*, vol. 17, no. 2, pp. 391–404, 2016.

[28] R. O. R. G. at the German Cancer Research Center, "Matrad," 2023.

[29] R. O. R. G. at the German Cancer Research Center, "matrad technical documentation," 2023.

[30] L. Hong, M. Goitein, M. Bucciolini, R. Comiskey, B. Gottschalk, S. Rosenthal, C. Serago, and M. Urie, "A pencil beam algorithm for proton dose calculations," *Physics in Medicine & Biology*, vol. 41, no. 8, p. 1305, 1996.

[31] H.-P. Wieser, E. Cisternas, N. Wahl, S. Ulrich, A. Stadler, H. Mescher, L.-R. Müller, T. Klinge, H. Gabrys, L. Burigo, *et al.*, "Development of the open-source dose calculation and optimization toolkit matrad," *Medical physics*, vol. 44, no. 6, pp. 2556–2568, 2017.

[32] A. Wächter and L. T. Biegler, "On the implementation of an interior-point filter line-search algorithm for large-scale nonlinear programming," *Mathematical programming*, vol. 106, pp. 25–57, 2006.

[33] L. Gurobi Optimization, "Gurobi algorithms," 2023.